

Testing Tidal-Torque Theory: I. Spin Amplitude and Direction

Cristiano Porciani^{1,2}, Avishai Dekel¹ and Yehuda Hoffman¹

¹*Racah Institute of Physics, The Hebrew University, Jerusalem 91904, Israel*

²*Institute of Astronomy, University of Cambridge, Madingley Road, Cambridge CB3-0HA, UK*

2 December 2024

ABSTRACT

We evaluate the success of linear tidal-torque theory (TTT) in predicting galactic-halo spin using a cosmological N -body simulation with thousands of well-resolved haloes. The proto-haloes are identified by tracing today’s haloes back to the initial conditions. The TTT predictions for the proto-haloes match, on average, the spin amplitudes of today’s virialized haloes if linear growth is assumed until $\sim t_0/3$, or 55–70 per cent of the halo effective turn-around time. This makes it a useful qualitative tool for understanding certain average properties of galaxies, such as total spin and angular-momentum distribution within haloes, but with a random scatter of the order of the signal itself. Non-linear changes in spin direction cause a mean error of $\sim 50^\circ$ in the TTT prediction at t_0 , such that the linear spatial correlations of spins on scales $\geq 1 h^{-1}\text{Mpc}$ are totally erased by non-linear effects. This questions the usefulness of TTT for predicting intrinsic alignments in the context of gravitational lensing. We find that the standard approximations made in TTT, including a second order expansion of the Zel’dovich potential and a smoothing of the tidal field, provide close-to-optimal results.

Key words: cosmology: dark-matter – cosmology: large-scale structure of Universe – cosmology: theory – galaxies: formation – galaxies: haloes – galaxies: structure

1 INTRODUCTION

Angular momentum is clearly one of the key physical ingredients in the process of galaxy formation. The total angular momentum, and its distribution, must have a crucial role in determining the galaxy history and final type. It has therefore been a subject for classical investigations, pioneered by Hoyle (1949), and then analysed qualitatively by Peebles (1969). This led to the ‘standard’ theory for the origin of angular momentum in the framework of hierarchical cosmological structure formation, the tidal-torque theory (TTT) due to Doroshkevich (1970) and White (1984).

Special interest in the subject has been revived recently because of a “spin crisis”, arising from cosmological simulations of galaxy formation which use hydrodynamical gravitational codes to follow the gas dynamics inside dark-matter haloes, and semi-analytical recipes for star formation and feedback. These simulations seem to yield luminous galaxies that are significantly smaller, and of much less angular momentum than observed disc galaxies (Navarro, Frenk & White 1995; Navarro & Steinmetz 1997, 2000). The discovery of massive black holes in galactic centers (Kormendy & Richstone 1995; Magorrian et al. 1998; Gebhardt et al. 2000a,b) provides another motivation for understanding the

detailed distribution of angular momentum within galaxies. A general need for a detailed recipe for the build-up of angular momentum in galaxies comes from the developing semi-analytic models, which have been proven very useful in the study of galaxy formation (e.g. White & Frenk 1991; Kauffmann, White & Guiderdoni 1993; Cole et al. 1994; Somerville & Primack 1999). Another current motivation comes from weak lensing studies. Our ability to reconstruct maps of the cosmic mass distribution from weak gravitational lensing measurements (Bacon, Refregier & Ellis 2000; Kaiser, Wilson & Luppino 2000; van Waerbeke et al. 2000, 2001; Wittman et al. 2000) is hampered by the unknown intrinsic distribution and alignment of galaxy shapes. As a first guess, one crudely assumes that the shapes and orientations of background galaxies are uncorrelated in space, and that the detected correlations of galaxy ellipticities are solely due to the lensing by the foreground mass distribution. However, a series of observations (Brown et al. 2000; Pen, Lee & Seljak 2000) and numerical simulations (Croft & Metzler 2000; Heavens, Refregier & Heymans 2000; Dekel et al. 2000) evidenced that both the intrinsic galaxy shapes and their spins are spatially correlated. Theoretical models for the alignment of disc galaxies orientations tend to as-

sume that they are induced by spin correlations (Catelan, Kamionkowski & Blandford 2001; Crittenden et al. 2001).

These issues add a timely aspect to the motivation for revisiting the classical problem of angular momentum, in an attempt to sharpen our understanding of its various components. This includes the first step of angular-momentum acquisition by dark haloes, which might be particularly assumed to be fairly well understood. The basic idea of TTT is that most of the angular momentum is being gained gradually by proto-haloes in the linear regime of density fluctuations growth, due to tidal torques from neighboring fluctuations, and that this process continues until the proto-halo reaches its maximum extent. The further assumption is that only little angular momentum is being exchanged between haloes later on in the non-linear regime, after the proto-haloes have decoupled from the expanding background and collapsed to virialized systems. It is commonly assumed that the baryonic material, which in general follows the dark-matter distribution inside each proto-halo, gains a similar specific angular momentum and carries it along when it contracts to form a luminous galaxy at the halo centre. This should allow us to predict galactic spins using the approximate but powerful analytic tools of quasi-linear theory of gravitational instability.

In a series of papers, we evaluate the performance of the TTT approximation, and trace the roles of its various ingredients, using a cosmological N -body simulation with thousands of well-resolved haloes. As we do so, we find to our surprise that some of the basic ingredients of TTT, which are commonly assumed to be of ‘text-book’ status, involve certain unjustified assumptions and confused understandings, which may lead to poor approximations. These papers represent attempts to clarify some of these controversial issues.

We address the TTT at different levels. In this paper (Paper I), we evaluate how well does the approximation predict the final angular momentum of a halo, given full knowledge of the corresponding initial proto-halo and the cosmological realization. In Paper II (Porciani, Dekel & Hoffman 2001), we attempt a deeper level of understanding of the origin of halo angular momentum, by investigating the relation between the different components of TTT. This study connects to the fundamental open question of how to identify a proto-halo in a given realization of initial conditions. In Paper III (Porciani & Dekel in preparation), we revise the standard scaling relation of TTT, based on the fact that the shear tensor is actually uncorrelated with the density contrast of the proto-halo (the density and shear being the trace and traceless parts of the same, deformation tensor). This scaling relation is used to predict the typical angular-momentum profile of haloes (Dekel et al. 2001; Bullock et al. 2001), and to provide a simple way to incorporate angular momentum in semi-analytic models of galaxy formation (Maller, Dekel & Somerville in preparation).

Given the initial conditions of a proto-halo and its environment, TTT predicts the final halo angular momentum based on four specific assumptions as follows: (a) The flow is laminar, with a one-to-one correspondence of Eulerian and Lagrangian positions, or the velocity field is properly smoothed such that laminarity prevails in practice. (b) The velocities obey the Zel’dovich approximation. (c) The potential at every point within the proto-halo can be approxi-

mated by its Taylor expansion to second order (with respect to spatial separation) about the centre of mass. (d) There is little contribution to the halo angular momentum from non-linear effects. In the current paper, we set to evaluate the global success of TTT in this task, and try to address the validity of each of the above assumptions. The role of non-linear effects, in particular, turns out to be the key issue. This will be an attempt to follow and improve on earlier work by White (1984), Hoffman (1986, 1988), Barnes & Efstathiou (1987), Catelan & Theuns (1996), Lee & Pen (2000) and Sugerman, Summers & Kamionkowski (2000).

The outline of this paper is as follows: In §2 we summarize the basics of linear tidal-torque theory. In §3 we describe the simulation and the halo finder. In §4 we describe the implementation of TTT to proto-haloes. In §5 we evaluate the success of TTT in predicting the amplitudes of halo spins. In §6 we assess the success of TTT in predicting the directions of halo spins. In §7 we address the spatial coherence of spin directions, which is directly relevant to intrinsic alignments in the context of gravitational lensing. In §8 we discuss our results and conclude.

2 TIDAL-TORQUE THEORY

We start by summarizing the basics of linear tidal-torque theory. The framework is the standard Friedmann-Robertson-Walker cosmological model in the matter-dominated post-recombination era, in which the matter is assumed to be a collision-less fluid and the dynamics is driven by gravity only. In the linear regime, the developing proto-haloes are assumed to be small perturbations about the mean universal density. The peculiar velocity field, due to the growing mode of gravitational instability, describes a potential flow with no curl, assuming that any primordial source of vorticity (e.g., due to some primordial turbulence, see Jones 1976) has decayed away due to the expansion of the universe.

Given a proto-halo, a patch of matter occupying an Eulerian volume γ that is destined to end up in a virialized halo, the goal is to compute the halo angular momentum about the centre of mass, to the lowest non-vanishing order in perturbation theory. The angular momentum at time t is defined by

$$\mathbf{L}(t) = \int_{\gamma} \rho(\mathbf{r}, t) [\mathbf{r}(t) - \mathbf{r}_{\text{cm}}(t)] \times [\mathbf{v}(t) - \mathbf{v}_{\text{cm}}(t)] d^3r, \quad (1)$$

where \mathbf{r} and \mathbf{v} are the position and peculiar velocity vectors, and the centre-of-mass quantities, \mathbf{r}_{cm} and \mathbf{v}_{cm} , are defined as usual. The term proportional to \mathbf{v}_{cm} does not contribute to \mathbf{L} , and it will not be considered any further. Re-write Eq. (1) in comoving units, $\mathbf{x} = \mathbf{r}/a(t)$ and $\mathbf{v} = a d\mathbf{x}/dt$, where $a(t)$ is the universal expansion factor, and replace $\rho(\mathbf{x}, t)$ with the density contrast $\delta(\mathbf{x}, t) = \rho(\mathbf{x}, t)/\bar{\rho}(t) - 1$ with respect to the average density $\bar{\rho}(t)$, to obtain

$$\mathbf{L}(t) = \bar{\rho}(t)a^5(t) \int_{\gamma} [1 + \delta(\mathbf{x}, t)] [\mathbf{x}(t) - \mathbf{x}_{\text{cm}}(t)] \times \dot{\mathbf{x}} d^3x. \quad (2)$$

A dot denotes a derivative with respect to cosmic time, t . In the matter-dominated era, $\bar{\rho}(t)a^3(t) = \bar{\rho}_0 a_0^3 = \text{const}$, where

the subscript 0 denotes quantities evaluated at the present time.

In the Lagrangian description of fluid dynamics, the comoving Eulerian position of each fluid element is given by its initial, Lagrangian position \mathbf{q} plus a displacement: $\mathbf{x}(\mathbf{q}, t) = \mathbf{q} + \mathbf{S}(\mathbf{q}, t)$. When fluctuations are small, or when the flow is properly smoothed, the mapping $\mathbf{q} \rightarrow \mathbf{x}$ is reversible and the flow is *laminar*. Then the Jacobian determinant $J = |\partial\mathbf{x}/\partial\mathbf{q}|$ does not vanish, and the continuity equation implies $1 + \delta[\mathbf{x}(\mathbf{q}, t)] = J^{-1}(\mathbf{q}, t)$. Substituting in Eq. (1) we obtain, for a laminar flow,

$$\mathbf{L}(t) = a^2(t) \bar{\rho}_0 a_0^3 \int_{\Gamma} [\mathbf{q} - \bar{\mathbf{q}} + \mathbf{S}(\mathbf{q}, t) - \bar{\mathbf{S}}] \times \dot{\mathbf{S}}(\mathbf{q}, t) d^3q, \quad (3)$$

where Γ is the region in Lagrangian space corresponding to γ in Eulerian space. Barred quantities are averages over \mathbf{q} in Γ . Note that Eq. (3) is exact in the absence of orbit crossing.

The displacement \mathbf{S} is now spelled out using the *Zel'dovich* approximation (Zel'dovich 1970), which is linear in Lagrangian terms and mildly non-linear in Eulerian space. It assumes that the proportionality between the velocity potential and the gravitational potential $\phi(\mathbf{q}, t)$, which holds in the linear regime for the growing mode of density fluctuations $\delta \propto D(t)$, can be extended into the mildly non-linear regime. This implies that the spatial and temporal dependences of \mathbf{S} can be decoupled,

$$\mathbf{S}(\mathbf{q}, t) = -D(t) \nabla\Phi(\mathbf{q}). \quad (4)$$

where $\Phi(\mathbf{q}) = \phi(\mathbf{q}, t)/4\pi G\rho(t)a^2(t)D(t)$ (with G Newton's gravitational constant). It also implies that the peculiar velocity and acceleration fields are parallel. Substituting Eq. (4) into Eq. (3) one obtains

$$\mathbf{L}(t) = -a^2(t)\dot{D}(t) \bar{\rho}_0 a_0^3 \int_{\Gamma} (\mathbf{q} - \bar{\mathbf{q}}) \times \nabla\Phi(\mathbf{q}) d^3q. \quad (5)$$

We see that the explicit growth rate is $L \propto a^2(t)\dot{D}(t)$. For an Einstein-de Sitter universe this is $\propto t$.^{*}

Next, assume that the potential is smoothly varying within the volume Γ , such that it can be approximated by its *second order* Taylor expansion about the centre of mass $\bar{\mathbf{q}}$,

$$\Phi(\mathbf{q}') \simeq \Phi(\mathbf{0}) + \frac{\partial\Phi}{\partial q'_i} \Big|_{\mathbf{q}'=\mathbf{0}} q'_i + \frac{1}{2} \frac{\partial^2\Phi}{\partial q'_i \partial q'_j} \Big|_{\mathbf{q}'=\mathbf{0}} q'_i q'_j, \quad (6)$$

where $\mathbf{q}' \equiv \mathbf{q} - \bar{\mathbf{q}}$.[†] Substituting in Eq. (5) one obtains the basic TTT expression for the i th Cartesian component:

$$L_i(t) = a^2(t)\dot{D}(t) \epsilon_{ijk} \mathcal{D}_{jl} I_{lk}, \quad (7)$$

where ϵ_{ijk} is the fully antisymmetric rank-three tensor, and the two key quantities are the *deformation* tensor at $\mathbf{q}' = \mathbf{0}$,

$$\mathcal{D}_{ij} = - \frac{\partial^2\Phi}{\partial q'_i \partial q'_j} \Big|_{\mathbf{q}'=\mathbf{0}}, \quad (8)$$

* A numerical integration of the cosmological relations shows that for all flat cosmologies the approximation $a^2\dot{D} \propto D^{3/2}$ holds to an excellent accuracy, and it deviates only slightly for open cosmologies.

† This is equivalent to assuming that the velocity field is well described by its linear Taylor expansion, i.e., $v_i - \bar{v}_i \simeq \mathcal{D}_{ij} q'_j$ (where v is in comoving units).

and the *inertia* tensor of Γ ,

$$I_{ij} = \bar{\rho}_0 a_0^3 \int_{\Gamma} q'_i q'_j d^3q'. \quad (9)$$

Note that only the traceless parts of the two tensors matter for the cross product in Eq. (7). These are the velocity *shear* or *tidal* tensor, $T_{ij} = \mathcal{D}_{ij} - (\mathcal{D}_{ii}/3)\delta_{ij}$, and the traceless quadrupolar inertia tensor, $I_{ij} - (I_{ii}/3)\delta_{ij}$. Thus, to the first non-vanishing order in perturbation theory, angular momentum is transferred to the developing proto-halo by the gravitational coupling of the quadrupole moment of its mass distribution with the tidal field exerted by neighboring density fluctuations. The torque depends on the proto-halo shape, the external tidal field, and the *misalignment* between the two. In particular, \mathbf{L} vanishes if Γ is a sphere or is bounded by an equipotential surface of Φ .

There is no *a priori* justification for truncating the expansion of the potential after second-order, Eq. (6). More generally, the expansion includes further terms,

$$\begin{aligned} L_i(t) &= L_i^{(2)}(t) + L_i^{(3)}(t) + \dots = \\ &= a^2(t)\dot{D}(t) \epsilon_{ijk} \left[\mathcal{D}_{jl} I_{lk} + \frac{1}{2} \mathcal{D}_{jlm}^{(3)} I_{lmk}^{(3)} + \dots \right], \end{aligned} \quad (10)$$

with

$$\mathcal{D}_{ijk}^{(3)} = - \frac{\partial^3\Phi}{\partial q'_i \partial q'_j \partial q'_k} \Big|_{\mathbf{q}'=\mathbf{0}}, \quad I_{ijk}^{(3)} = \bar{\rho}_0 a_0^3 \int_{\Gamma} q'_i q'_j q'_k d^3q'. \quad (11)$$

Here, multipole moments of a given order of the proto-halo mass distribution are coupled with spatial derivatives of the same order of the potential. This is a consequence of the $1/r^2$ scaling of gravitational interactions, and indeed, the total torque for a localized charge in an external electrostatic field admits a similar expansion (e.g., Jackson 1975, exercise 4.5). Note that dipole interactions [i.e., terms proportional to $\mathbf{p} \times \mathbf{g}(\mathbf{q}' = 0)$ with \mathbf{p} the mass dipole moment and \mathbf{g} the gravitational acceleration] do not contribute to the torque because the spin is considered in the centre-of-mass frame, where the mass dipole vanishes. On the other hand, dipole interactions are expected to play an important role in the evolution of orbital angular momentum.

After the dark-matter haloes have detached from the expanding background and collapsed into condensed systems, the tidal torquing continues, but at a highly reduced rate. Peebles (1969) estimated the typical torque exerted on a quadrupolar mass distribution by a population of point-like galaxies, showing that the transfer of angular momentum becomes less and less efficient with time. This is a consequence of the fact that haloes become small when they collapse, as well as the fact that they tend to move away from each other due to the Hubble expansion.

3 SIMULATION AND HALO FINDING

The N -body simulation analysed here was performed as part of the GIF project (e.g., Kauffmann et al. 1999) using the parallel, adaptive particle-particle/particle-mesh (AP³M) code developed by the Virgo consortium (Pearce et al. 1995; Pearce & Couchman 1997). As an example, we use a simulation of the τ CDM scenario, in which the cosmology is flat,

Einstein-de Sitter with density parameter $\Omega_m = 1$, and Hubble constant $H_0 = 100 h \text{ km s}^{-1} \text{ Mpc}^{-1}$ with $h = 0.5$. The power spectrum of initial density fluctuations is CDM with shape parameter $\Gamma = 0.21$. The amplitude of the power spectrum is set such that the rms overdensity in top-hat spheres of radius $8 h^{-1} \text{ Mpc}$, as extrapolated using linear theory to the present epoch, is $\sigma_8 = 0.51$.[‡]

The simulation was performed in a periodic cubic box of side $84.55 h^{-1} \text{ Mpc}$, with the mass represented by 256^3 particles of $1.0 \times 10^{10} h^{-1} M_\odot$ each. Long-range gravitational forces were computed on a 512^3 mesh, while short-range interactions were calculated as in Efstathiou & Eastwood (1981). At late times ($z \lesssim 3$), the corresponding gravitational potential asymptotically matches a Plummer law with softening $\epsilon = 36 h^{-1} \text{ kpc}$ both at large and small scales. The simulation started at a redshift $z = 50$ and ended at the present time, $z = 0$. The initial conditions were generated by displacing particles according to the Zel'dovich approximation from an initial stable 'glass' state (e.g. White 1996). More details are given in Jenkins et al. (1998).

We identify virialized dark-matter haloes at $z = 0$ as follows. First, we select an initial set of groups of particles using a friends-of-friends method (e.g., Davis et al. 1985) with a linking length $b = 0.2$ in units of the average inter-particle distance. This algorithm identifies regions bounded by a surface of approximately constant density contrast, $\rho/\bar{\rho} \simeq 3/(2\pi b^3)$ (e.g. Cole & Lacey 1996). Assuming that the density profiles of these groups approximate singular isothermal spheres, the selection criterion can be expressed in terms of the average density contrast in the halo, $\rho/\bar{\rho} \simeq 9/(2\pi b^3)$. Thus, $b = 0.2$ corresponds to haloes with a mean density contrast $\simeq 179$, in general agreement with the predictions of the spherical collapse model for perturbations whose outer shells have collapsed recently.

We then remove unbound particles from each halo by the following iterative procedure. At each step, we compute the energies of all particles in the current centre-of-mass frame, and remove the most unbound particle. We then recompute the energies of all the particles and so on. The iteration stops when no unbound particles are found. Note that a particle that has been removed is allowed to re-enter the halo if it becomes bound at a later step due to changes in the position and velocity of the centre of mass. Clumps which end up containing between 100 and 200 particles loose, on average, ~ 5.5 per cent of their mass as unbound particles. In a few cases, typical of small haloes, the friends-of-friends algorithm identifies 'fake' haloes which are not bound gravitationally. For example, seven friends-of-friends haloes (out of ~ 7300) composed by more than 100 particles end up containing only 10 bound particles or less after the un-binding procedure. More massive haloes are, naturally, less

[‡] Such a power spectrum may arise, for example, if a late decay of massive τ neutrinos produces an additional background of relativistic e and μ neutrinos, thus delaying the onset of matter domination and lowering the effective value of Γ (Bond & Efstathiou 1991; Efstathiou, Bond & White 1992; White, Gelmini & Silk 1995). Here it simply serves us as a scenario which obeys many of the observational constraints from large-scale structure, including the normalizations set by cluster abundance and by COBE's measurements of large-angle anisotropies in the CMB, independently of its physical origin.

affected by unbound interlopers because their potential wells are typically deeper. For instance, the mean fraction of unbound mass removed from clumps which end up containing between 200 and 1000 (1000-3000) particles is ~ 2.9 per cent (~ 2.0 per cent). In the following we consider only haloes which contain more than 100 particles after the un-binding procedure is applied. Our conclusions regarding TTT turn out to be insensitive to the removal of unbound particles, and to increasing the minimum-mass threshold. In order to try to restrict ourselves to galactic haloes, we also exclude all the ~ 200 haloes which consist of more than 3000 particles – these tend to have more substructure and are likely to correspond to groups or clusters of galaxies.

The robustness of our conclusions regarding TTT with respect to the halo-finding algorithm (e.g., friends-of-friends versus fitting a spherical or ellipsoidal density profile, Bullock et al. 2000) is investigated in another paper in preparation. Note that all the haloes in our current sample are not subclumps of larger host haloes, for which linear theory is not expected to be valid. This excludes about 10 per cent of the haloes that are more massive than $10^{12} h^{-1} M_\odot$ (Sigad et al. 2001).

4 IMPLEMENTING TTT

The proto-halo regions Γ in Lagrangian space are defined straightforwardly by tracing all the halo particles into their Lagrangian positions. Generally, most of the proto-halo mass is contained in a simply connected Lagrangian region, but in some cases the proto-halo may be divided into several compact regions which are connected by thin filaments. Nearly 10 per cent of the proto-haloes are characterized by extended filaments departing from a compact core.

We stress that the proto-haloes at earlier times are defined solely based on their identification as virialized haloes at $z = 0$, without worrying about the details of the merger history, and without applying any other criteria at the initial conditions. Some of the results reported below are specific to this choice of considering all today's halo particles at all times rather than, e.g., investigating the history of the halo major progenitor (Klypin et al., in preparation; Wechsler et al., in preparation).

For each proto-halo, we compute the Lagrangian inertia tensor by direct summation over its N particles of mass m each:

$$I_{ij} = m \sum_{n=1}^N q_i^{(n)} q_j^{(n)}, \quad (12)$$

with $\mathbf{q}^{(n)}$ the position of the n -th particle with respect to the halo centre of mass.

We use three alternative methods to measure the shear tensor at the proto-halo centre of mass in the initial conditions of the N -body simulation.

Method 1, top-hat smoothing: We smooth the gravitational potential used to generate the initial Zel'dovich displacements, and then differentiate it two times with respect to the spatial coordinates to obtain the deformation tensor. Smoothing is done using a top-hat window function, while derivatives are computed on a grid. The top-hat smoothing radius in comoving units, R_{th} , is taken to be defined by $(4\pi/3)\bar{\rho}_0 R_{\text{th}}^3 = M$, with M the virial halo mass. This is the

only practical method for application in analytic and semi-analytic modelling of galaxy formation. We refer to it as the *standard* method of TTT.

Method 2, fit total: The smoothing applied in Method 1 is associated with a loss of information. First, the coarse-graining procedure averages over small-scale structure. Second, the spherical smoothing kernel does not maintain the details of the proto-halo shape, since, as we find in Paper II, most proto-halos are far from being spherically symmetric. We minimize smoothing in the computation of the tidal tensor in the following way. The comoving linear velocity field, in the proto-halo centre-of-mass frame, is expanded in terms of the corresponding Eulerian comoving separation, \mathbf{x} , as

$$v_i = \mathcal{D}_{ij} x_j . \quad (13)$$

The components of the deformation tensor $\mathcal{D}_{ij} = \partial v_i / \partial x_j$ are computed by least-squares fitting to the simulation data (cf. Kaiser 1991). This is realized by solving the system of equations

$$\begin{aligned} \sum_{n=1}^N \mathcal{D}_{ik} x_k^{(n)} x_i^{(n)} &= \sum_{n=1}^N v_i^{(n)} x_i^{(n)} , \\ \sum_{n=1}^N [\mathcal{D}_{ik} x_k^{(n)} x_j^{(n)} + \mathcal{D}_{jk} x_k^{(n)} x_i^{(n)}] &= \sum_{n=1}^N [v_i^{(n)} x_j^{(n)} + v_j^{(n)} x_i^{(n)}] . \end{aligned} \quad (14)$$

Since the linear growing mode of the gravitational velocity field is curl-free, Eq. (14) has been derived after imposing the condition $\mathcal{D}_{ij} = \mathcal{D}_{ji}$. We then compute the symmetric, traceless shear tensor $T_{ij} \equiv \mathcal{D}_{ij} - (1/3)\mathcal{D}_{ii}\delta_{ij}$. The shear field computed this way corresponds to minimal smoothing, at the level of the individual particles in the N -body simulation. However, even though no velocity averaging is performed, method 2 is, in some sense, similar to using a smoothing kernel which adapts itself to the proto-halo shape. The resulting T_{ij} describes the quadrupolar structure of the velocity field in the proto-halo at the particle level. Method 2 is therefore expected to provide better predictions for \mathbf{L} than Method 1 whenever the top-hat smoothing is associated with a severe loss of information.

Method 3, fit external: The interactions between particles that belong to the same proto-halo cannot create any net angular momentum. This motivates us to consider the shear tensor generated solely by the density perturbations lying outside the proto-halo volume, Γ . This is realized by decomposing the linear velocity field into two parts, $\mathbf{v} = \mathbf{v}^{(\text{self})} + \mathbf{v}^{(\text{ext})}$, accounting for the gravitational pull of the mass lying in and outside the proto-halo, respectively. In practice, for each particle in Γ , we first compute the linear gravitational acceleration generated at $z = 50$ by all the other point masses forming the proto-halo. From this quantity, we then subtract the acceleration caused by the same particles as if they were part of a uniform background. This is computed using the unperturbed particle positions of the glass state which, formally, correspond to $z \rightarrow \infty$. Rescaling the result we obtain $\mathbf{v}^{(\text{self})}$. The difference between the actual velocity of the particles in the simulation at $z = 50$ and this “self” gravitationally induced term is taken to represent $\mathbf{v}^{(\text{ext})}$. Indeed, our estimate for $\mathbf{v}^{(\text{ext})}$ generates, in practice, the same spin as the total velocity field. Eventually, the ex-

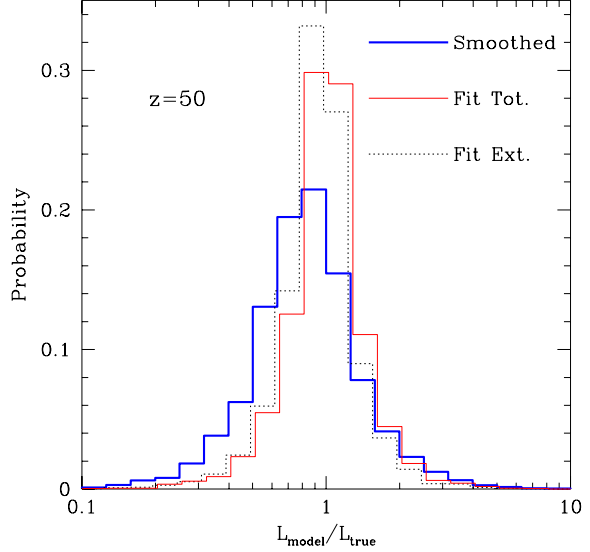


Figure 1. Predicted versus actual angular-momentum amplitude at the initial time, $z = 50$. Shown is the distribution over all the haloes in our sample. The three histograms correspond to the different methods of computing the shear tensor discussed in the main text (§4): using top-hat smoothing (thick line) or fitting with no smoothing of either the total shear (thin line) or the external part only (dotted line). To improve readability, the thin and dotted histograms have been slightly displaced in the horizontal direction.

ternal tidal field is computed by least-squares fitting. Note that, since $\mathcal{D}_{ij}^{(\text{self})} \propto I_{ij}$, the self field does not contribute to the angular momentum also at a linear level – i.e. there is no self-torquing.

The results obtained by Method 2 and Method 3 contain spurious contributions due to errors in the determination of the deformation tensor by the fit of a linear model to a discrete set of points. However, since the external shear is expected to vary more smoothly than the self gravity on a proto-halo scale, $\mathcal{D}_{ij}^{(\text{self})}$ should be described more accurately by the linear expansion of the velocity field. For this reason, Method 3 should provide a better estimate of the angular momentum. Note, however, that additional noise is introduced in Method 3 by replacing the uniform background density distribution with the glass state.

5 SPIN AMPLITUDE

Given a proto-halo at the initial conditions, we first investigate the performance of TTT, Eq. (7), in terms of predicting the amplitude of the halo angular momentum. Any systematic deviation of the mean predicted amplitude from that obtained in the simulations can be eliminated by adjusting the effective time near turn-around at which the linear TTT growth is assumed to stop. Random deviations, both due to the approximations made already at the initial conditions as well as non-linear effects at late epochs, cannot be avoided and should be estimated.

We start by testing the accuracy of TTT in the linear regime, at the *initial* time, $z = 50$. For each halo, we

compute the inertia tensor I_{ij} and the shear tensor T_{ij} using the three different methods described in §4. We then compute the amplitude L_{model} as predicted by Eq. (7), and compare it with the actual angular momentum of the protohalo particles, L_{true} . The distribution of the ratio of the two over the protohaloes is shown in Fig. 1, and characterized in Table 1. The mean (median) values for methods 1, 2, 3 are 0.95 (0.83), 1.05 (0.99), 1.01 (0.95) respectively. In all cases the probability distribution is positively skewed, and is leptokurtic (with a sharp peak and long tails) with respect to a Gaussian distribution in log-space. It is therefore not very useful to quantify the dispersion about the mean by a single standard deviation, so we quote instead the 68.3 per cent confidence interval, obtained by locating the values corresponding to the 15.9 and 84.2 percentiles in the cumulative distribution. For methods 1, 2, 3 we find (0.53, 1.28), (0.72, 1.31), (0.71, 1.24) respectively. As a single measure of scatter we use half the 68.3 per cent range, which is 0.37, 0.29, 0.26 respectively. All three methods involve the second-order truncation of the expansion of the potential and some smoothing. These are the only sources of error, since the Zel'dovich approximation is exact at the initial conditions of the simulation by construction. Even though the cases with minimum smoothing (methods 2 and 3) involve noisy fits of the small-scale structure, they give somewhat more accurate predictions. The external fit does just a little better than the total fit, both in terms of systematic error and scatter. However, the smoothed tidal field (method 1), which is the only practical method for semi-analytic modelling of galaxy formation, also leads to a small systematic deviation of the mean, of only ~ 5 per cent. The scatter, though, is of the order of the signal for all three methods already at the initial conditions.

These numbers change only slightly when restricting the analysis to the very well-resolved haloes containing 1000 particles or more. In this case, the mean (median) of the distribution of the amplitude ratio is 0.90 (0.79), 1.06 (1.02), 1.02 (0.98) for methods 1, 2, 3 respectively. The corresponding scatter is 0.32, 0.30, 0.27.

When we add the *third-order term* in the Taylor expansion of the gravitational potential, i.e., the second term in the right-hand side of Eq. (11), we find no significant improvement in the systematic error and in the scatter. In this case the mean (median) and scatter of $L_{\text{model}}/L_{\text{true}}$ are 0.95 (0.83) ± 0.36 , almost identical to the second-order results (top-hat smoothing is adopted in both cases). A more detailed inspection reveals the following. When considering only those haloes for which standard second-order TTT over-predicts or under-predicts the spin amplitude by more than a factor of 3, we find that by adding the third-order term one improves the prediction in about 75 per cent of the cases, though the overall scatter increases. In the case of severe over-prediction, the mean (median) and scatter are 4.54 (3.41) ± 0.44 for second-order TTT and 3.81 (2.63) ± 0.79 for third-order TTT. In the case of severe under-prediction, the numbers are 0.25 (0.26) ± 0.07 for second-order TTT and 0.40 (0.33) ± 0.16 for third-order TTT. On the other hand, when the second-order TTT predictions are reasonably good, the addition of the third-order term makes no general improvement. For the haloes where the prediction is within 30 per cent of the true value, the mean (median) and scatter are 0.94 (0.92) ± 0.17 for second-order TTT and 0.94

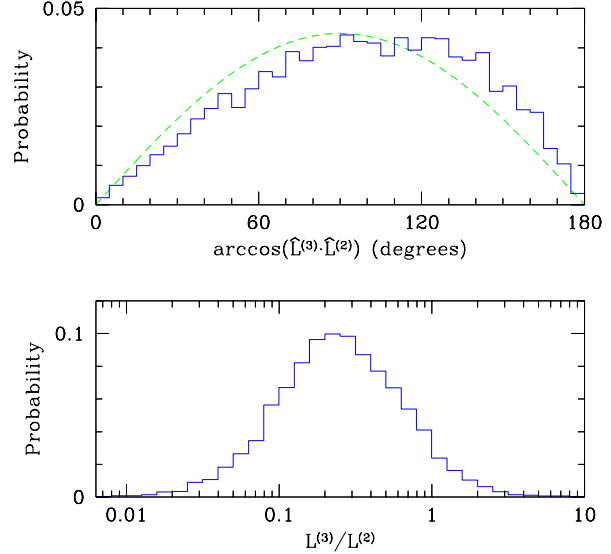


Figure 2. Probability distributions for the angle (top) and the ratio of the amplitudes (bottom) between the halo spin predicted by TTT considering the first term on the right hand side of Eq. (11), $\mathbf{L}^{(2)}$, and the second term, $\mathbf{L}^{(3)}$. The dashed line in the top panel is the expected distribution for random orientations.

(0.91) ± 0.21 for third-order TTT. Part of the failure of the third order term to improve the results in these cases could be attributed to numerical errors in the computation of the third-order term, which are particularly important when the high-order corrections are small.

Fig. 2 shows the distribution of the angle between the direction of \mathbf{L} as predicted by standard second-order TTT (top-hat smoothing) and by the third-order term alone. We see that the additional contribution points at an almost random direction compared to the leading-order term, with an average angle of 98° and a scatter of $\sim 45^\circ$. Fig. 2 shows the distribution of the corresponding amplitude ratio, $L^{(3)}/L^{(2)}$, with an average of 0.39 and a scatter of 0.27. These indicate that any truncation of the expansion is doomed to introduce an error that is not negligible compared to the signal. We conclude that the second-order expansion is the most sensible and practical procedure, but it is associated with a noticeable error.

In the second step of our testing, we address the growth rate indicated by TTT in the *quasi-linear* regime, $L \propto a^2 \dot{D}$. We do it by comparing for each proto-halo the model and true L values at $z = 3$, where the fluctuations are still linear on the Lagrangian scale of the protohaloes, but the protohalo substructures, and maybe even the haloes themselves, already involve non-linear fluctuations. We show in Fig. 3 the distribution of the ratio L_{model} to L_{true} for standard TTT. We show, for comparison, the corresponding distribution for the case where the model angular momentum is computed directly from the $z = 3$ velocities, as predicted by the Zel'dovich approximation from the initial conditions with the corresponding growth.

The deviation of the ZA histogram from a Dirac δ function at unity reflects the deviation of the angular-momentum growth rate from the linear prediction, $L \propto a^2 \dot{D}$. It does

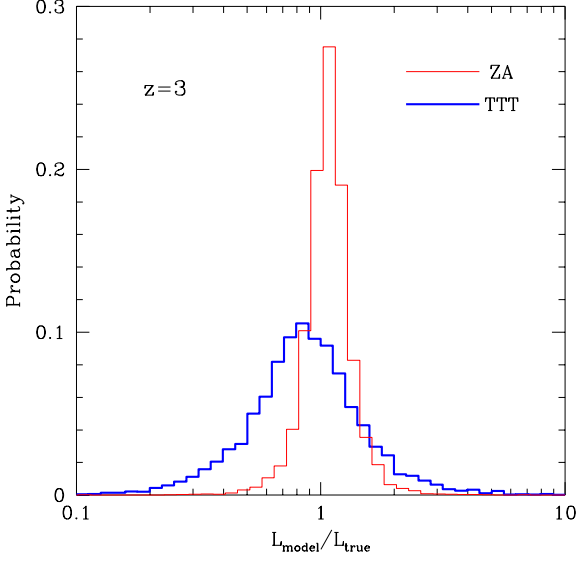


Figure 3. Model versus true angular-momentum amplitudes in the quasi-linear regime, $z = 3$. Shown is the distribution over all the haloes in our sample. The thick histogram corresponds to standard TTT based on the truncated and smoothed shear tensor. The thin histogram (which has been slightly shifted to the right) corresponds to L computed directly from the $z = 3$ Zel’dovich velocities. The deviations from unity in the latter is solely due to the non-linear effects in the growth rate of angular momentum.

not involve the errors associated with the smoothing and the truncation of the potential because the initial conditions also obey the Zel’dovich approximation. The predicted growth rate is slightly higher than the true growth rate, but the corresponding 8 per cent systematic overestimate and the 0.19 scatter are relatively small. The additional effects of truncation plus smoothing in TTT are responsible for the larger scatter in the TTT histogram. In this case, the systematic error is only 2 per cent, due to a slight systematic underestimate by TTT of the spin amplitude at $z = 50$, which partly compensates for the overestimate of the growth rate. Note, however, that the median of the distribution (see Table 1) keeps roughly constant between $z = 50$ and $z = 3$. The scatter of 0.43 is comparable to the signal, and is slightly larger than the initial scatter of 0.38 due to the deviations from the linear growth rate.

In the third step, we compare the spin amplitudes at $z = 0$, after non-linear processes have affected the true spin. We first wish to determine the effective time in each halo history, or on average for all haloes, at which the linear growth of angular momentum à la TTT should be assumed to stop in order to obtain the best prediction for its amplitude at $z = 0$. Then, we wish to evaluate the scatter about the mean TTT result.

In order to learn about the actual evolution in the non-linear regime, we show in Fig. 4 the distribution over the haloes of the ratio between L_{true} at $z = 0$ ($t = t_0$) and at $z = 3$ ($t = t_0/8$). The actual growth factor between these times has a mean value of 2.9 (with a scatter of ~ 1.4), which implies that the linear growth should be stopped at an effective time $2.9 t_0/8 \simeq 0.36 t_0$ (or $z \simeq 1$). This time is somewhat

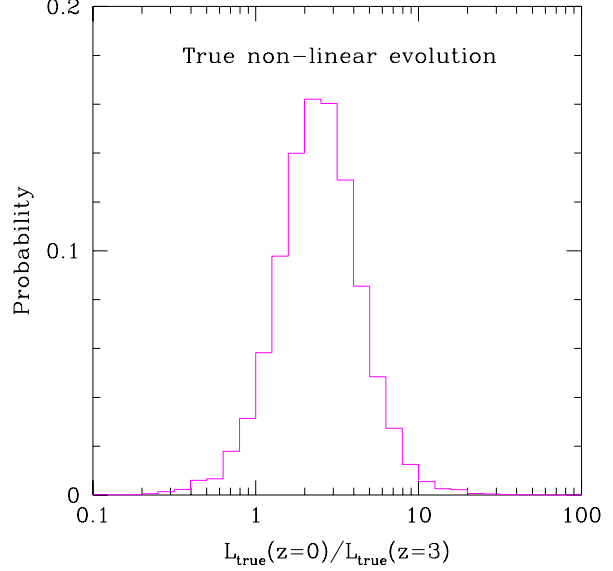


Figure 4. True growth factor of angular momentum between $z = 3$ and $z = 0$. Shown is the distribution over all the haloes in our sample.

earlier than maximum expansion for the outer shell of the halo (using the terminology of the spherical collapse model), because our haloes, by definition, have their outermost shells reaching virialization today, and were therefore at maximum expansion at $t \simeq t_0/2$ (or $z \simeq 0.6$). Linear growth until maximum expansion would have implied a growth factor of 4 instead of 2.9 since $z = 3$.

The actual evolution of spin amplitudes of the simulated haloes is shown in Fig. 5. The average and scatter refer alternatively to the ratio of $L(t)$ and the initial proto-halo spin, and the ratio of $L(t)$ and the final halo spin. We see that, in agreement with the results shown in Fig. 4, the best effective time for stopping the TTT growth is $\sim 0.3 t_0$. This would properly adjust the mean, but would leave a significant scatter from halo to halo as indicated by the error bars.

In Fig. 6, we show the distribution of the ratio of model to true L values at $z = 0$, with the TTT growth stopped in three different ways. In the top panel, the TTT growth of each halo has been stopped at a fixed fraction of its turnaround time t_{ta} , as predicted by the spherical collapse model based on the value of the initial density fluctuation smoothed on the scale of the proto-halo (namely, the time at which the linearly extrapolated density contrast is $\delta = 1.06$). By stopping the TTT growth for each halo at $t_{\text{TTT}} = 0.56 t_{\text{ta}}$, the median of the ratio $L_{\text{model}}/L_{\text{true}}$ becomes unity. Alternatively, in the central panel, the TTT growth for each halo has been stopped at a fixed fraction of the time t_{1D} when the smoothed proto-halo is predicted by the Zel’dovich approximation at the initial conditions to collapse along the first principal axis of the deformation tensor. Requiring that the median of the corresponding amplitude ratio is equal to unity gives $t_{\text{TTT}} = 0.39 t_{1D}$. In the bottom panel, the linear spin growth has been stopped at the same epoch for all the haloes, $t_{\text{TTT}} = 0.35 t_0$ corresponding to $z = 1.03$, which has been determined again to bring the median value

Table 1. Characteristics of the distribution of the ratio of amplitudes of the spins as predicted by the model and as measured in the simulations. Listed are the mean and several percentiles, as well as the scatter as measured by half the central 68.3 per cent region. TTT=tidal-torque theory, NB= N -body simulations, ZA=Zel'dovich approximation.

Comparison	z	Fig.	Mean	2.5%	15.9%	50%	84.2%	97.5%	Scatter
TTT/NB	50	1	0.95	0.27	0.53	0.83	1.28	2.48	0.37
TTT(2)/NB	50	1	1.05	0.43	0.72	0.99	1.31	2.12	0.29
TTT(3)/NB	50	1	1.01	0.41	0.71	0.95	1.24	1.98	0.26
ZA/NB	3	3	1.08	0.65	0.87	1.05	1.25	1.67	0.19
TTT/NB	3	3	1.02	0.27	0.53	0.86	1.39	2.73	0.43
NB/NB $\times 100$	50/0	-	1.17	0.26	0.52	0.96	1.72	3.33	0.60
NB/NB	3/0	-	0.50	0.13	0.23	0.41	0.72	1.41	0.24
NB/NB	1.2/0	-	1.05	0.32	0.55	0.90	1.45	2.76	0.45
NB/NB	0.6/0	-	1.19	0.46	0.75	1.08	1.53	2.72	0.39
NB/NB	0.2/0	-	1.08	0.65	0.90	1.04	1.23	1.70	0.16
NB/NB	0/3	4	2.93	0.70	1.38	2.41	4.26	7.89	1.44
ZA/NB	0	6a	1.68	0.28	0.61	1.20	2.39	5.44	0.89
ZA/NB	0	6b	1.64	0.32	0.66	1.23	2.39	5.17	0.86
ZA/NB	0	6c	1.47	0.33	0.66	1.22	2.16	4.19	0.75
TTT/NB	0	6a	1.41	0.21	0.48	1.00	2.04	4.91	0.78
TTT/NB	0	6b	1.38	0.24	0.52	1.00	2.03	4.75	0.76
TTT/NB	0	6c	1.28	0.23	0.51	1.00	1.92	4.18	0.70

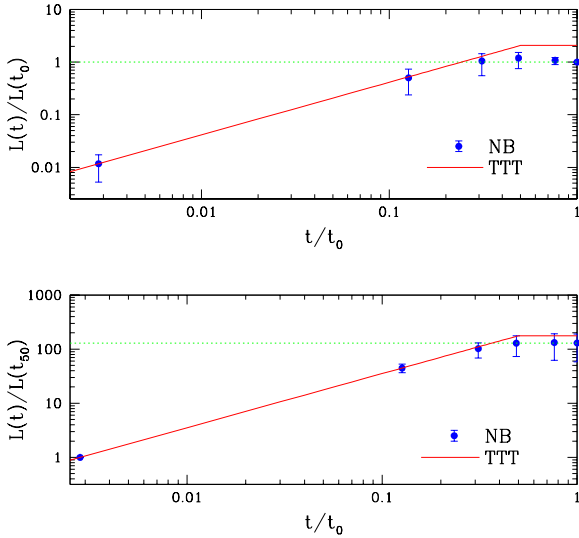


Figure 5. True evolution of spin amplitude in the simulation compared to TTT. Shown are the average and the 68.3 per cent confidence interval over the haloes at different times, of the ratio of spin amplitude $L(t)$ and either the spin today (top panel) or the spin at the initial conditions (bottom panel). The continuous lines represent the linear TTT growth stopped at maximum expansion ($t = 0.5 t_0$). The dotted lines mark the average value at t_0 .

of $L_{\text{model}}/L_{\text{true}}$ to unity. As at $z = 3$, we show the histograms for TTT and for the pure Zel'dovich velocities at t_{TTT} . The corresponding percentiles are listed in Table 1. Note that, despite the different stopping times, the three probability distributions are very similar; the 68.3 per cent

confidence level corresponds to a factor of 2 random error. The histograms for TTT and for the pure Zel'dovich velocities show a similar scatter, indicating that the choice of t_{TTT} is the dominant factor in determining the scatter compared to the other approximations involved in TTT.

The impression from Fig. 5 that the growth of spin amplitude really stops at some specific epoch is somewhat misleading. When we investigate halo by halo, we find that about 38 per cent of our haloes actually loose angular momentum between $z = 0.6$, $z = 0.2$ and $z = 0$ due to non-linear interactions (see a similar finding by Sugerman et al. 2000). On average, these haloes loose ~ 30 per cent of their spin between $z = 0.6$ and $z = 0$. This is partly a result of considering in each proto-halo the same group of particles at all times, based on their association with a halo at $z = 0$. Angular momentum from these proto-halo particles may be transferred to outer shells of matter. Mergers, tidal encounters and the presence of substructure all contribute to angular-momentum transfer. This decrease of L with time at late epochs indicates that in many case the TTT growth actually continued roughly until turn-around, stopped, and started declining thereafter. This is one of the reasons for why the effective time for stopping the TTT growth should be somewhat before turn-around.

Some fraction of the haloes have their spin growing also at late epochs: about 21 per cent of our spins grow between $z = 0.6$, $z = 0.2$ and $z = 0$. On average, these haloes increase their spin by ~ 60 per cent between $z = 0.6$ and $z = 0$. However, for about 57 per cent of our haloes the evolution of spin amplitude in the non-linear regime is weak, less than 20 per cent between $z = 0.6$ and $z = 0$, in pleasant agreement with the concept of TTT. Considering the whole halo population, we find that the mean value and the scatter of the ratio $L(z = 0.6)/L(z = 0)$ are 1.19 and 0.39 – or 1.01 and 0.34 for the inverse ratio. We conclude that

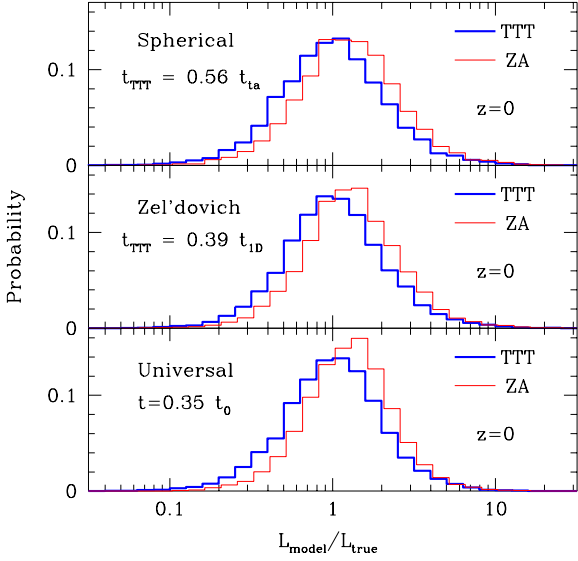


Figure 6. Model versus true spin amplitudes in the non-linear regime, at $z = 0$. The TTT growth has been stopped at t_{TTT} such that the median of the ratio $L_{\text{model}}/L_{\text{true}}$ is unity. In the top panel $t_{\text{TTT}} = 0.56 t_{\text{ta}}$, a fixed fraction of the turn-around time as predicted for each halo by the spherical-collapse model based on the smoothed initial density fluctuation. In the middle panel $t_{\text{TTT}} = 0.39 t_{1D}$, a fixed fraction of the time of orbit crossing along the first principal axis of the deformation tensor as predicted by the Zel'dovich approximation based on the smoothed initial conditions. In the bottom panel, the linear spin growth has been stopped at the same epoch for all haloes, $t_{\text{TTT}} = 0.35 t_0$. The thick histogram corresponds to standard TTT, with a scatter of a factor of two. The thin histogram (which has been slightly displaced to the right) corresponds to L_{model} computed directly from the Zel'dovich velocities at t_{TTT} ; it does not involve the approximations made in TTT at the initial conditions and can be interpreted as reflecting only the scatter due to the choice of t_{TTT} .

even though non-linear effects do not significantly change the average amplitude of halo spins, the variety of evolutionary paths result in a large scatter about the mean TTT prediction at $z = 0$.

The bottom line is that standard TTT provides a successful order-of-magnitude estimate for the halo angular-momentum amplitude. If TTT growth is stopped at turn-around, the systematic overestimate of the final spin is of the order of the signal. This systematic overestimate is removed if the TTT growth is stopped at about 56-70 per cent of the turn-around time, or about 23-35 per cent of the collapse time, depending on how these times are defined. However, the random scatter from halo to halo is of the order of the signal itself. Part of this scatter is due to real non-linear evolution, reflected in an uncertainty in the choice of the effective time at which the TTT growth should be stopped, and part is due to the approximations involved in applying TTT already at the initial conditions. The standard truncation of the potential and smoothing of the shear tensor is close to the best one can do in TTT.

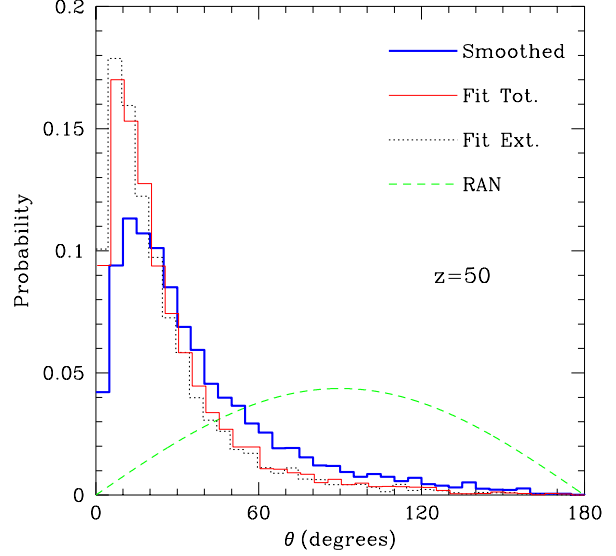


Figure 7. The distribution of angles between model and true spin directions in the linear regime, $z = 50$. The three histograms (slightly shifted horizontally to improve readability) correspond to the different methods of computing the shear tensor (§4). The dashed line is the expected distribution for random orientations. The misalignment is due to the truncation of the Taylor expansion of the potential. Additional error is added by the smoothing on the proto-halo scale.

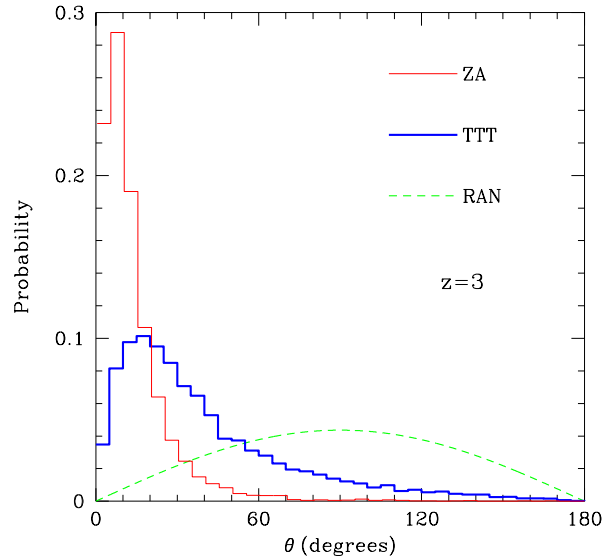


Figure 8. The distribution of the angles between model and true spin directions in the quasi-linear regime, at $z = 3$. The thick histogram is for the standard, truncated and smoothed TTT. The thin histogram (which has been slightly displaced to the right) is for the angular momentum derived from the Zel'dovich velocities, i.e., its predicted direction at any time is the true spin direction at $z = 50$. The deviation of this Zel'dovich histogram from perfect alignment reflects weak non-linear temporal variations in the spin directions. The dashed curve is the distribution of angles in the case of random orientations.

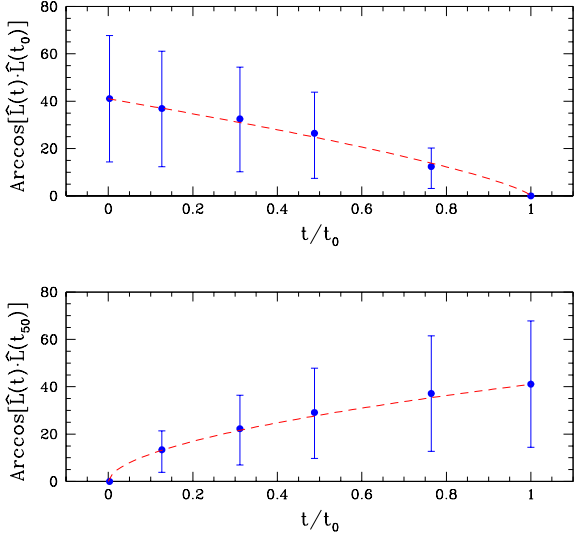


Figure 9. Evolution of true spin direction. Shown are the average and the 68.3 per cent confidence interval over the haloes of the angle between the angular momentum at time t and its counterpart evaluated either at the present time (t_0 , top panel) or at the initial conditions (t_{50} , bottom panel). Linear TTT predicts perfect alignment. The dashed lines show empirical functional fits: $41^\circ(1 - t/t_0)^{0.75}$ and $41^\circ(t/t_0)^{0.55}$ respectively.

6 SPIN DIRECTION

The fact that the TTT prediction of the spin amplitude is only good to order of magnitude raises doubts about the prospects of TTT as a predictor for the direction of the spin vector, because a random error of a few tens of percents in each component is likely to be associated with a non-negligible loss of information about the direction. We compare the predicted and true directions of the spin vector for each halo via the distribution of the angle θ between them over the haloes, proceeding from the linear regime at $z = 50$, to the quasi-linear epoch $z = 3$, and to the present non-linear epoch $z = 0$, as we did for the spin amplitude.

In Fig. 7 we compare the three methods of computing the shear tensor (§4) at the initial conditions, $z = 50$. Zel’dovich velocities would have corresponded to a Dirac δ function at $\theta = 0^\circ$, while a random distribution of relative directions would correspond to the distribution shown by a dashed line. The average angle of misalignment in the linear regime is 37° , 26° , and 25° for methods 1, 2, and 3, respectively. The corresponding scatter (defined, as before, as half the 68.3 per cent confidence interval) is $\sim 26^\circ$, 18° , and $\sim 18^\circ$ in the three cases. Other percentiles of these distributions are given in Table 2. As in the case of the amplitude, the sources of misalignment in the linear regime are the second-order truncation of the potential and the smoothing. Considering only the haloes with 1000 particles or more, we obtain only slightly smaller misalignments, with mean values of 33° , 24° , 23° and scatter of 24° , 17° , 15° for the three methods, respectively.

We find that considering the third-order term in the expansion of the gravitational potential within the proto-halo region (method 1, not shown in the figure) results in a

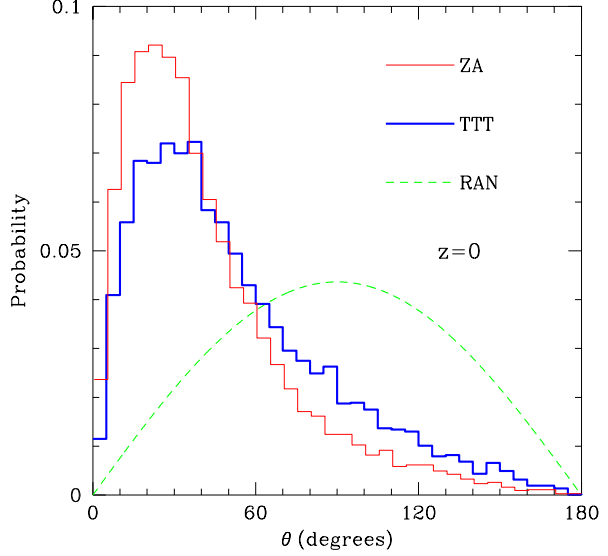


Figure 10. As in Fig. 8, but at $z = 0$. The distribution of angles between the true spin directions at $z = 3$ and $z = 0$ (not shown) practically coincides with the thin histogram, which measures the non-linear temporal variations in spin direction.

very small improvement: the average is reduced from 37° to 34° , and the scatter from 26° to 24° . Considering the haloes for which standard TTT does a poor job and mispredicts the spin direction by more than 60° , we find that by adding the third-order term one improves the prediction in 70 per cent of the cases. For the remaining haloes, where TTT is doing a relatively reasonable job, the third-order term does not lead to a general improvement and it improves the prediction in only 54 per cent of the cases.

It is interesting to check, already in the linear regime, whether a good prediction for the spin direction is associated with a good prediction for the spin amplitude. For this purpose, we split the halo sample into a “good” group and a “bad” group according to whether the spin direction predicted by standard TTT and the true spin direction differ by less or more than 30° , containing 54 and 46 per cent of the haloes respectively. For the “good” group, the average and 68.3 per cent confidence interval of $L_{\text{model}}/L_{\text{true}}$ are 0.91 and (0.58, 1.18), and for the “bad” group they are 1.00 and (0.44, 1.44). We learn that erroneous predictions for the spin direction correspond to a large scatter in the amplitude, while more accurate predictions for the direction tend to systematically underestimate the amplitude. We find that for 31 per cent of our haloes, the TTT estimates lie both within 30° of the true direction and differ from the correct amplitude by less than 30 per cent.

The goodness of TTT predictions correlates with the halo mean specific angular momentum. For instance, considering the 10 per cent of the haloes with the lowest specific angular momentum, we find that standard TTT overestimates the spin amplitude by an average (median) factor of 1.6 (1.22) with a scatter of ± 0.92 , and mispredicts the spin direction by 67° (60°) $\pm 40^\circ$. On the other hand, for the 10 per cent of the haloes with the highest specific angular momentum, we find that the mean (median) and scatter

Table 2. Characteristics of the distributions of the angle between the vectors of the spins as predicted by the model and as measured in the simulations. Listed are the mean and several percentiles, as well as the scatter as measured by half the central 68.3 per cent region. TTT=tidal-torque theory, NB= N -body simulations, ZA=Zel’dovich approximation.

Comparison	z	Fig.	Mean	2.5%	15.9%	50%	84.2%	97.5%	Scatter
TTT/NB	50	7	36.8	3.9	11.0	27.3	63.5	123.6	26.2
TTT(2)/NB	50	7	25.8	2.3	7.1	18.1	43.8	99.1	18.3
TTT(3)/NB	50	7	24.7	2.3	6.6	17.0	41.7	95.5	17.6
ZA/NB	3	8	13.4	1.3	3.9	9.6	21.4	48.6	8.7
TTT/NB	3	8	40.1	4.1	12.3	30.3	69.9	129.0	28.8
NB/NB	50/0	-	41.1	5.1	14.4	33.1	67.7	122.6	26.6
NB/NB	3/0	-	36.9	4.5	12.3	29.1	61.1	116.3	24.4
NB/NB	1.2/0	-	32.5	3.5	10.2	24.3	54.4	111.8	22.1
NB/NB	0.6/0	-	26.4	2.6	7.4	18.7	43.8	100.3	18.2
NB/NB	0.2/0	-	12.4	1.1	3.1	7.9	20.2	52.1	8.5
NB/NB	0/3	-	36.9	4.5	12.3	29.1	61.1	116.3	24.4
ZA/NB	0	10	41.1	5.1	14.4	33.1	67.7	122.6	26.6
TTT/NB	0	10	52.2	7.1	18.7	43.3	89.0	139.3	35.1

are $0.87 (0.83) \pm 0.24$ for the amplitude ratio and $18^\circ (13^\circ) \pm 11^\circ$ for the angle. These statistics vary continuously as a function of the halo specific angular momentum. A similar behaviour is found using methods 2 and 3 of §4, but in these cases TTT does not introduce a systematic error for the haloes with the highest specific angular momentum. This behaviour seems to suggest that TTT introduces a typical angular-momentum error per particle, and good predictions can be only obtained when the halo mean specific angular momentum is larger than this typical uncertainty.

In Fig. 8 we test how well the spin maintains the constant direction implied by TTT during the quasi-linear evolution, until $z = 3$. The spin derived from the Zel’dovich velocities at $z = 3$, which is of course parallel to the spin at the initial conditions, has an average misalignment with the true spin of only 13° with a comparable scatter. This small misalignment implies that the spin tends to keep a pretty fixed direction during quasi-linear evolution. When this small temporal variation of the angle is convolved with the truncation and smoothing involved in applying TTT to the initial conditions, the misalignment becomes more significantly larger, with an average of 40° and a scatter of $\sim 30^\circ$. The mean evolution and scatter of the true halo spin direction all the way to $z = 0$ is summarized in Fig. 9, either relative to the direction at $z = 0$ or relative to the direction at $z = 50$. Empirical functional fits are $41^\circ (1 - t/t_0)^{0.75}$ and $41^\circ (t/t_0)^{0.55}$ respectively. We see a significant true misalignment developing due to non-linear effects.

Fig. 10 addresses the full non-linear variation of spin direction down to $z = 0$. When the model spin is computed from the particles following the Zel’dovich approximation, we obtain the true total misalignments due to non-linear effects, as in Fig. 9, with an average and scatter of 41° and 27° . This true misalignment occurs mostly between $z = 3$ and $z = 0$: this part of the misalignment (not shown in the figure) has an average and scatter of 37° and 24° , almost as large as the total true misalignment.

Finally, the full TTT prediction, with the additional

truncation and smoothing, yields a mean misalignment with the actual spin at $z = 0$ of 52° with a scatter of $\sim 35^\circ$. We see that most of the misalignment is due to true non-linear evolution of spin direction. This implies that no matter how exactly TTT is applied, it is doomed to be a limited predictor of spin direction in the non-linear regime.

The bottom line is that non-linear evolution causes significant variations in spin direction, which limit the quality of linear TTT as an accurate predictor of spin direction. Still, there is a significant correlation between the direction predicted by TTT and the final spin direction.

7 SPIN–SPIN CORRELATIONS

TTT has been used to predict spatial spin correlations as indicators of intrinsic spatial alignments of galaxies in the context of interpreting weak gravitational lensing signals (Catalan et al. 2001; Crittenden et al. 2001). Our results of the previous section already indicate that TTT is a poor predictor of galaxy spin direction. In order to address directly the usefulness of TTT as a predictor of spatial spin correlations, we compute in this section two-point spin statistics.

A summary of the relevance to lensing studies is as follows. A shear signal, interpreted as a result of gravitational lensing due to the large-scale distribution of matter, has been detected by several groups (Bacon et al. 2000; Kaiser et al. 2000; van Waerbeke et al. 2000, 2001; Wittman et al. 2000). Lensing shear maps can be used to directly reconstruct the mass distribution, free of galaxy biasing. However, a significant uncertainty arises due to possible intrinsic coherent alignment of galaxy shapes. Indeed, Brown et al. (2000) (see also Pen et al. 2000) claim to have detected a non-vanishing correlation between galaxy ellipticities in the local universe, over a range of angular separations between 1 and 100 arc-minutes. Since the galaxy samples used for these studies are relatively nearby, a lensing interpretation is highly improbable, so this signal is likely to reflect intrinsic galaxy alignments.

The simplest theoretical approach is to link galaxy shapes to halo spins by assuming that galaxy discs are perpendicular to the spin vector of their host haloes. The spins are expected to be correlated because the tidal field, that plays a key role in generating the angular momentum, is expected to have a non-negligible coherency over large scales (Catelan & Porciani 2001). Alternative models assume that the light profile of elliptical galaxies approximate the shape of their hosting haloes (Croft & Metzler 2000; Heavens et al. 2000).

We introduce two statistics for measuring two-point spin correlations. The two-point correlation function of spin directions is simply,

$$\eta(r) = \langle \hat{L}(\mathbf{x}) \cdot \hat{L}(\mathbf{x} + \mathbf{r}) \rangle. \quad (15)$$

The function

$$\eta_2(r) = \langle [\hat{L}(\mathbf{x}) \cdot \hat{L}(\mathbf{x} + \mathbf{r})]^2 \rangle - \frac{1}{3} \quad (16)$$

measures the correlation of spin axes independent of the sense of rotation, and is therefore more directly relevant to the intrinsic correlations of shape orientations that mimic lensing signal.

In Fig. 11 we compare the functions $\eta(r)$ and $\eta_2(r)$, at different epochs of the simulation, with the prediction of TTT as evaluated from the initial density and velocity fields.[§] We see in the simulation that at high redshift there is a positive spin–spin correlation at separations of a few comoving megaparsecs, but the correlation signal on these scales completely disappears by $z = 0$. This is mainly due to non-linear effects. On the other hand, the TTT approximation maintains the same correlation function at all times, because it keeps the spin directions fixed, by construction. At $z = 50$, TTT matches well the simulation data, and since it always builds upon the initial conditions, it maintains a correlation signal at late times as well. The linear TTT approximation naturally fails to include the non-linear effects that weaken the correlations on any given scale, and it thus overestimates the correlation at late times.[¶]

The weakening of the correlation signal on the scales shown can be attributed to two non-linear effects. First, the members of galaxy pairs tend to get closer due to the evolving clustering. Second, the spin directions themselves evolve away from the TTT predictions. As a result of the first effect, the linear correlation signal simply shifts to smaller scales. The interpretation of the second could be that non-linear dynamics erases the linear spin-spin correlations on all scales, while non-linear halo-halo interactions build up a new correlation signal on small scales. We distinguish between these

[§] The correlation functions presented by Heavens et al. (2000) and by Croft & Metzler (2000) seem to be less noisy than ours, but this is an illusion caused by the fact that they allowed haloes smaller than we do, down to 10 particles, while the resolution of their simulations is similar to ours. By including more haloes in the sample, one may be tempted to assume that the statistical errors are reduced, but the error budget must include the very large errors associated with measuring spin and shape for each halo based on such a small number of particles (see Bullock et al. 2001).

[¶] We also find that adding the third term in the Taylor expansion of the potential – see Eq. (11) – leaves the prediction for the correlation functions almost unaffected (not shown in the figure).

effects by also showing in Fig. 11 the spin-spin correlation functions as computed using the TTT predictions for the halo spins but located at the actual halo positions at $z = 0$. Even though this model does a better job than linear TTT, it still over-predicts the correlations measured in the simulations at $z = 0$. This demonstrates that non-linear halo-halo interactions and angular-momentum exchanges with additional infalling material play an important role in determining spatial spin correlations on small scales. Using a simulation of higher resolution, one can indeed detect significant spin correlations at $z = 0$ on scales below $0.4 h^{-1} \text{Mpc}$ (Dekel et al. 2000).

In summary, at late times, TTT tends to over-predict the spin–spin correlations of non-linear dark-matter haloes by a factor of a few. However, TTT may still be somewhat relevant because the spin direction of discs today may, in fact, be determined by the spin directions of their parent haloes at higher redshift, where the correlations are larger. On the other hand we know that this is true only for the haloes that we selected at $z = 0$, and we do not know whether this is still valid for the subhaloes which host disc formation at higher redshift.

8 CONCLUSION

We have evaluated the performance of linear tidal-torque theory in predicting the spin of galactic haloes using ~ 7300 well-resolved virialized dark-matter clumps extracted from a cosmological N -body simulation. We defined haloes in today’s density field using the standard friends-of-friends algorithm, but it would be useful for future work to check robustness to alternative halo finders as well as to different cosmological scenarios.

We found that, for a given proto-halo at the initial conditions, TTT provides a successful order-of-magnitude estimate of the final halo spin amplitude. The TTT prediction matches on average the spin amplitude of today’s virialized haloes if linear TTT growth is assumed until about $t_0/3$, or about 5/9 of the turn-around time for each halo. The random error, from halo to halo, is about a factor of two. This makes TTT useful for studying certain aspects of galaxy formation, such as the origin of a universal spin profile in haloes (Bullock et al. 2001; Dekel et al. 2001), but only at the level of average properties.

Non-linear evolution causes significant variations in spin direction, which limit the accuracy of the TTT predictions to a mean error of $\sim 50^\circ$. Furthermore, spatial correlations of spins on scales $\geq 1 h^{-1} \text{Mpc}$ are totally erased by non-linear effects. This limits the usefulness of TTT in predicting intrinsic galaxy alignments in the context of weak gravitational lensing (Catelan et al. 2001; Crittenden et al. 2001). This situation may improve if the orientations of today’s discs were determined by the halo spins at a very high redshift, which are better described by TTT. On the other hand, we know this only for the haloes selected at $z = 0$, and not necessarily for the subhaloes which host disc formation at higher redshifts. A study of this effect would require a high-resolution simulation in which a detailed galaxy formation scheme is incorporated.

For practitioners of TTT, we found that the standard approximations made in TTT, such as the second order ex-

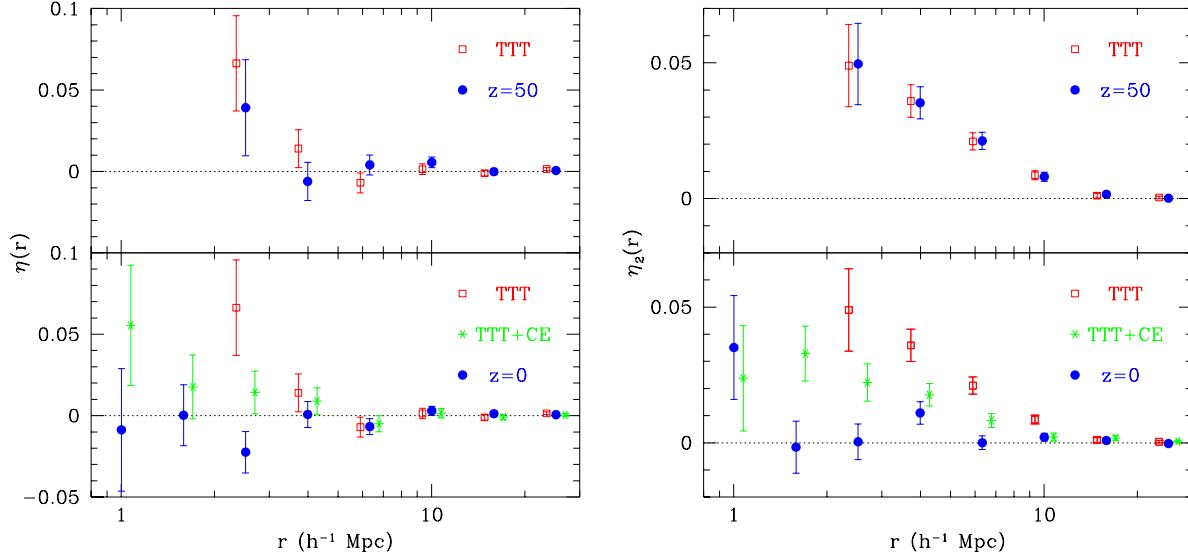


Figure 11. Spin–spin correlation functions, as defined in Eq. (15) (left) and Eq. (16) (right). The time-independent TTT predictions (open squares) are compared with the true simulation data (filled circles) at $z = 50$ (top) and $z = 0$ (bottom). The effect of allowing for clustering evolution (CE) by associating the TTT predictions with the halo positions at $z = 0$ is also shown (stars). The TTT predictions were artificially displaced by ± 0.03 in $\log(r)$ for clarity. Error-bars denote one standard deviation. The spatial separation r is in comoving units

pansion of the Zel’dovich potential, and the smoothing of the shear tensor on the proto-halo scale, are hard to improve upon. The inaccuracies in the TTT predictions are dominated by real non-linear effects rather than the above approximations.

In order to deepen our understanding of how TTT actually works, we investigate in paper II the cross-talk between the proto-halo inertia tensor and the external shear tensor. We find to our surprise that they are strongly correlated, in the sense that their minor, major and medium principal axes tend to be aligned, in this order. This means that the angular momentum, which plays such a crucial role in the formation of disc galaxies, is only a residual which arises from the little, ~ 10 per cent deviations from perfect alignment of T and I . We find there that the $T - I$ correlation induces a weak tendency of the proto-halo spin to be perpendicular to the major axis of T , but non-linear changes in spin direction erase any memory of the initial shear tensor, and therefore observed spin directions cannot serve as very useful indicators for the initial shear tensor (cf. Lee & Pen 2000).

On the other hand, the strong $T - I$ correlation investigated in Paper II provides a promising hint for how to solve a long-standing problem in galaxy formation theory, of identifying the boundaries of proto-haloes in cosmological initial conditions (Porciani, Dekel & Hoffman, in preparation).

In our studies of the cross-talk between the different components of TTT, we have also realized another surprise that leads to a revision in the standard scaling relation of TTT (White 1984). We find in Paper III (Porciani & Dekel in preparation) that the off-diagonal, tidal terms of the deformation tensor, which drive the torque, are hardly correlated with the diagonal terms, which determine the overdensity at the proto-halo centre. The latter enters the TTT

scaling relation via the expected collapse time of the proto-halo, and the lack of correlation with the torque leads to a modification in the scaling relation. The revised scaling relation can be applied shell by shell, together with an extended Press-Schechter recipe for merger history, in order to explain the origin of the universal angular-momentum profile of haloes (Bullock et al. 2001; Dekel et al. 2001). It can also be very useful in incorporating spin in semi-analytic models of galaxy formation (Maller, Dekel & Somerville in preparation).

ACKNOWLEDGMENTS

This research has been partly supported by the Israel Science Foundation grant grants 546/98 (AD) and 103/98 (YH), and by the US-Israel Binational Science Foundation grant 98-00217 (AD). CP acknowledges the support of a Golda Meir fellowship at HU and of the EC RTN network ‘The Physics of the Intergalactic Medium’ at the IoA. We thank our GIF collaborators, especially H. Mathis, A. Jenkins and S.D.M. White, for help with the GIF simulations.

REFERENCES

- Bacon D.J., Refregier A.R., Ellis R.S., 2000, MNRAS, 318, 625
- Barnes J., Efstathiou G., 1987, ApJ, 319, 575
- Bond J.R., Efstathiou G., 1991, Phys. Lett. B, 265, 245
- Brown M.L., Taylor A.N., Hambly N.C., Dye, S., 2000, MNRAS, submitted, astro-ph/0009499
- Bullock J.S., Kolatt T.S., Sigad Y., Somerville R.S., Kravtsov A.V., Klypin A.A., Primack J.R., Dekel A., 2000, MNRAS, in press, astro-ph/9908159

- Bullock J.S., Dekel A., Kolatt T.S., Kravtsov A.V., Klypin A.A., Porciani C., Primack J.R., 2001, *ApJ*, submitted, astro-ph/0011001
- Catelan P., Porciani C., 2001, *MNRAS*, 323, 713
- Catelan P., Theuns T., 1996, *MNRAS*, 282, 436
- Catelan P., Kamionkowski M., Blandford R., 2001, 320, L7
- Cole S., Lacey C., 1996, *MNRAS*, 281, 716
- Cole S., Aragon-Salamanca A., Frenk C.S., Navarro J.F., Zepf S.E., 1994, *MNRAS*, 271, 781
- Crittenden R.G., Natarajan P., Pen U., Theuns T., 2001, *ApJ*, in press, astro-ph/0009052
- Croft, R.A.C., Metzler C.A., 2000, *ApJ*, 545, 561
- Davis M., Efstathiou G., Frenk C.S., White S.D.M., 1985, *ApJ*, 292, 371
- Dekel A., Bullock J.S., Porciani C., Kravtsov A.V., Kolatt T.S., Klypin A.A., Primack J.R., 2000, in J.G. Funes S.J., E.M. Corsini, eds. *Galaxy Disks and Disk Galaxies*, ASP Conference Series, astro-ph/0011002
- Doroshkevich A.G., 1970, *Astrofizika*, 6, 581
- Efstathiou G., Eastwood J.W., 1981, *MNRAS*, 194, 503
- Efstathiou G., Bond J.R., White S.D.M., 1992, *MNRAS*, 258, L1
- Gebhardt K., et al., 2000a, *ApJ*, 539, L13
- Gebhardt K., et al., 2000b, *ApJ*, 543, L5
- Heavens A., Refregier A., Heymans C., 2000, 319, 649
- Hoffman Y., 1986, *ApJ*, 301, 65
- Hoffman Y., 1988, *ApJ*, 329, 8
- Hoyle F., 1949, Burgers J.M., van de Hulst H.C., eds., in *Problems of Cosmical Aerodynamics*, Central Air Documents Office, Dayton, p. 195
- Jackson J.D., 1975, *Classical Electrodynamics*, Wiley, New York
- Jenkins A. et al. 1998, *ApJ*, 499, 20
- Jones B.J.T., 1976, *Rev. Mod. Phys.*, 1976, 48, 107
- Kaiser N., 1991, *ApJ*, 366, 388
- Kaiser N., Wilson G. & Luppino G.A., 2000, *ApJ letters*, submitted, astro-ph/0003338
- Kauffmann G., White S.D.M., Guiderdoni B., 1993, *MNRAS*, 264, 201
- Kauffmann G., Colberg J.M., Diaferio A., White S.D.M., 1999, *MNRAS*, 303, 188
- Kormendy J., Richstone D., 1995, *ARA&A*, 33, 581
- Lee J., Pen U., 2000, *ApJ*, 532, L5
- Magorrian J., et al., 1998, *AJ*, 115, 2285
- Navarro J.F., Frenk C., White S.D.M., 1995, *MNRAS*, 275, 56
- Navarro J.F., Steinmetz M., 1997, *ApJ*, 478, 13
- Navarro J.F., Steinmetz M., 2000, *ApJ*, 538, 477
- Pearce F.R., Couchman H.P.M., 1997, astro-ph/9703183
- Pearce F.R., Couchman H.P.M., Jenkins A.R., Thomas P.A., 1995, *Hydra-Resolving a Parallel Nightmare*, in *Dynamic Load Balancing on MPP systems*
- Peebles P.J.E., 1969, *ApJ*, 155, 393
- Pen U., Lee J., & Seljak U., 2000, *ApJ*, 543, 107
- Somerville R.S., Primack J.R., 1999, *MNRAS*, 310, 1087
- Sugerman B., Summers F.J., Kamionkowski M., 2000, *MNRAS*, 311, 762
- van Waerbeke L. et al. , 2000, *A&A*, 358, 30
- van Waerbeke L. et al. , 2001, *A&A*, submitted, astro-ph/0101511
- White M., Gelmini M., Silk J. 1995, *Phys. Rev. D*, 51, 2669
- White S.D.M., 1984, *MNRAS*, 286, 38
- White S.D.M., 1996, Schaeffer R., Silk J., Spiro M., Zinn-Justin J., eds., in *Cosmology and Large-scale Structure*, Elsevier, Dordrecht, The Netherlands, p. 349
- White S.D.M., Frenk C.S., 1991, *ApJ*, 379, 52
- Wittman D.M., Tyson J.A., Kirkman D., Dell'Antonio I., Bernstein G., 2000, *Nature*, 405, 143
- Zel'dovich Ya.B., 1970, *A&A*, 5, 84

This paper has been produced using the Royal Astronomical Society/Blackwell Science L^AT_EX style file.